Buoyancy-driven exchange flow between two adjacent building zones connected with top and bottom vents

S. Nabi[1], M.R. Flynn

Department of Mechanical Engineering, University of Alberta, Edmonton, AB, Canada T6G 2G8

Abstract

We examine the buoyancy driven flow between two adjacent building zones separated by top and bottom vents with and without a source of buoyancy. In the absence of a source, by opening the vents, the pressure difference between the two zones drives the exchange flow. When there is an isolated source of buoyancy, two distinct flow regimes are defined: a ventilation-dominated regime in which the flow that is generated by the initial temperature difference, and a source-dominated regime in which the flow is principally governed by the source. Here, we restrict attention to the former case. Thus in each zone our analytical model assumes a horizontal interface that separates the upper layer, which is comprised of fluid having the initial density of the light zone, from the lower layer, comprised of fluid whose density is larger than that of the light zone. The transient evolution of such interfaces along with the stratification and buoyancy in each zone are predicted. Attention is focused on the influence of the effective area, source buoyancy flux and the time during which the source is switched on. Because the interface elevations change significantly at early times, a non-monotonic behavior is predicted for the evolution of stratification in the light zone. We also find that the terminal stratification and buoyancy in both zones are not impacted by the number of connecting vents; however, this number has a strong influence on how quickly steady state is achieved. Similitude laboratory experiments help to corroborate key predictions.

Keywords: buoyancy-driven exchange flow, Boussinesq flow, Natural ventilation, Displacement ventilation, Similitude experiments, filling-box process

List of variables

a	area of a single vent	α	entrainment coefficient
A^*	Effective vent area	F_s	Source buoyancy flux
b	non-dimensional buoyancy	ρ	density (kg/m^3)

[1] Corresponding author email: nabi@ualberta.ca (Now at Mitsubishi Electric Research Laboratories, Cambridge, MA 02139)

Symbol	Description	Symbol	Description
D	vent diameter (m)	ρ_{00}	reference density (kg/m^3)
g'	reduced gravity (m^2/s)	ℓ	lock length (m)
h	distance between the top of the top vent and ceiling (m)	H, L, W	height, length and width of the rooms (tank), respectively (m)
$h_b(t)$	depth of the interface ascending in light zone (m)	$Q(t,z)$, $M(t,z)$, $F(t,z)$	volume (m^2/s), momentum (m^3/s^2) and buoyancy (m^3/s^3) flux within plume, respectively
$h_t(t)$	depth of the interface descending in dense zone (m)	u_1, h_1	dense gravity current velocity (m/s) and depth (m), respectively
N	Number of vents	u_2, h_2	internal bore velocity (m/s) and depth (m), respectively
$Q_e(t)$	exchange volume flux per unit width (m^2/s)	x, z	horizontal and vertical coordinates (m)
t	time (s)	$\rho_a(t,z)$, $\Delta_a(t,z)$	density (kg/m^3) and reduced gravity (m/s^2) of the ambient, respectively
t_2	time taken for the internal bore to reach the doorway (s)	T_E	characteristic draining time
t_E	ending time (s)	Π_s	Source strength defined in (28)
t_3	time taken for the first front to reach the top of the vent (s)	$U(t,z)$	velocity of the descending layers in the dense zone ambient (m/s)

Subscripts/Superscripts

Symbol	Description	Symbol	Description
0	dense zone	c	light zone
b, t	Bottom and top	f	final

1 Introduction

Buoyancy-driven exchange flow is a common phenomenon in many different situations, such as environmental (e.g. river plumes), architectural (e.g. natural ventilation) and industrial (e.g. fire protection) settings 1 [1-6]. While much attention has been given to exchange flow between (semi-)infinite or infinite regions and finite regions, less is known regarding the exchange flow between inter-connected finite regions [7-11]. This lack of knowledge limits the

deployment of natural ventilation, which is a potentially viable ventilation strategy in many geographical regions. Expanding the reach of natural ventilation is desirable because of the energy savings associated with a reduced reliance on traditional HVAC equipment. Hence, a better understanding of natural ventilation, with a potential to balance all or part of the energy consumed by such equipment, is an imperative task for engineers and architects.

Two major perspectives can be identified to describe air flow in buildings: macroscopic and microscopic [2]. In the former, the building is idealized as a collection of finite-size control volumes to solve for bulk quantities while in the latter approach the conservation equations are applied to describe the details of many important parameters related to internal and external flows within and around buildings such as temperature, velocity, etc. Multizone and well-mixed models are examples of the macroscopic method while detailed analytical methods or Computational Fluid Dynamics (CFD), which resolves conservation of mass, momentum and energy and, if applicable, turbulent closure models, are among the microscopic approaches.

Multizone network models are able to predict mass and energy exchange flow rates much faster compared to CFD models, especially when the number of connected rooms is large. However, multizone models assume a stationary system and thereby ignore momentum conservation in calculating bulk properties. They are therefore suitable for determining properties at steady state but much less so when modeling transient adjustments [2]. Furthermore, multizone models neglect zonal stratification considering, instead, each zone to be well-mixed [11]. To overcome this limitation, which is especially severe when a strong vertical thermal stratification is anticipated Wang and Chen [12] proposed to couple multizone models with a CFD data and observed improvements when compared with experimental data [13].

Stratification can also be included by applying so-called zonal models. Here, the building zone is divided into a number of homogenous subzones, whose number is much less than the number of grid points in a typical CFD simulation [14]. In this way it is feasible to study air flow for a large number of rooms. For instance, Song et al. [3] presented a case study for a 18-zone building. They

3

assessed mixing by numerically computing the mean age of air and used their results to improve the sub-zoning procedure. However, this approach needs extra information and/or models to define the flow. Moreover, and consistent with multizone models, in the zonal model the momentum equation is not resolved. To overcome this, further improvements are needed which may increase the computational cost as high as a CFD simulation [4].

Currently, computational fluid dynamics (CFD) models are used extensively in the analysis of airflow. Tan and Glicksman [15] presented a strategy to couple multizone modes with CFD to improve predictions of natural ventilation flow behavior and also model fidelity for both buoyancy-driven and wind-driven flows in large multi-storey buildings. Laughman et al. [5] used CFD to simulate refrigerant dispersion in single and connected rooms. They observed that the exchange of flow between two zones or between a single zone and the exterior is highly dependent on the location and size of the vents. They also reported the existence of horizontal currents with a velocity that can be scaled by analytical gravity current models.

The application of CFD to whole-building design has been limited as it requires excessive computer resources and long run times [4]. The computational cost is of course more problematic when a time-critical simulation or a fast on-demand prediction is desired [16]. In this paper, we focus on analytical models which we later validate by comparison with the data from similitude experiments. Better understanding of analytical models, which include momentum equation and also take the zonal stratification into account as opposed to multizone models, can be also helpful to better improve methods based on Fast Fluid Dynamics, FFD [17], which rely on thermal plume models.

Linden et al. [7] developed an analytical model describing displacement ventilation in a single room connected to the exterior via top and bottom vents. The room was forced by a single steady heat source located at ground level. The steady state consists of two layers of uniform, but different, densities that are separated by a sharp interface whose height can be computed from the vent sizes and room height.

An integral component of Linden et al.'s analysis is the modeling of turbulent convection using the plume theory originally developed by Morton et al. [18]. Although Morton et al.'s theory was developed for the case of a plume rising through infinite ambient, subsequent researchers adapted these results to the case of a "filling-box" flow consisting of a plume rising in a room. In this scenario, fluid which has been in the plume soon spreads out along the ceiling and modifies the ambient, and due to re-entrainment, this ambient fluid changes the behavior of the plume. Thus, a time-dependent solution which takes into account the interaction between the buoyant plume and the evolving ambient is required. Baines and Turner's [19] approach consisted of solving the plume/ambient conservation of mass, momentum and density deficiency equations asymptotically and thereby describing the late time stratification assuming that the buoyancy inside the control volume increases linearly in time. Worster and Huppert [20] further developed the model due to Baines and Turner [19] and presented an approximate analytical expression for the density profile in a filling box as it evolves with time.

In both the works of Worster and Huppert [20] and Baines and Turner [19] however, the source is assumed to be ideal, i.e. the source volume flux is zero. In many real problems, the source of buoyancy may also involve a source of mass. Germeles [21] introduced a numerical scheme to solve the governing equations for both the plume and the ambient, in the case of such a non-ideal plume. His approach gives the ambient density profile as a function of depth and time. Caulfield and Woods [8], using Germeles's numerical scheme, have considered the flow within an enclosed space with a single vent and a local "hot spot".
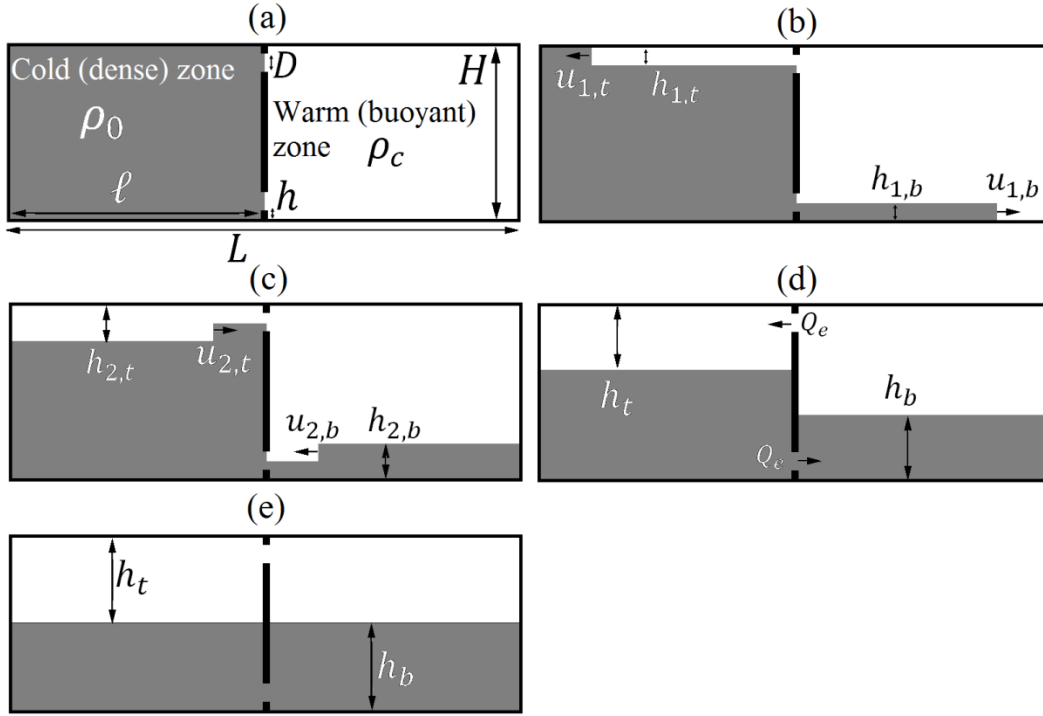
Figure 1. Schematic of the displacement exchange flow in the absence of source at (a) $t = 0$, the instant when buoyancy-driven motion begins, (b) $t < t_{1,b}$ and $t_{2,b}$, before the dense or light gravity currents reach the end wall, (c) $t < t_{2,b}$ and $t_{2,t}$, after reflection of the dense and light gravity currents as internal bores, (d) $t > t_{2,b}$ and $t_{2,t}$, after the dense and light bores reach the horizontal position of the vents, $x = \ell$ and (e) $t = t_E$ when the exchange flow is terminated.

Most previous work on natural ventilation has been restricted to a single space. In the architectural case, however, buildings rarely are single interior spaces. On the contrary, buildings are typically characterized by multiple rooms and corridors. This study extends the research analytical and experimental works by Nabi and Flynn [10], Linden et al. [7] and Nabi and Flynn [11] to analyze the transient buoyancy-driven flows between two connected chambers. As discussed in Linden [22], buoyancy-driven exchange flows highly depend on the position of the interior vents. Previously, we examined the exchange flow between two zones of slightly different densities separated by a single common doorway which was located at the bottom of each zone [10, 11]. In order to gain a more complete understanding of architectural exchange flows, we now extend our investigation to cases where the bottom openings or vents are matched by an equal or unequal number of vents adjacent to the ceiling, which we will hereafter refer to as the top vents. The number of bottom and top vents we denote by N_b and N_t, respectively,

each has a diameter D. The volumetric exchange rate is Q_e and, in order to satisfy volume conservation, must be equal in magnitude as regards the flow through the bottom and top vents. Geometrical parameters, such as H, h, ℓ and L are defined in Figure 1. We assume a symmetrical building h is also the distance between the top of the top vent and the ceiling.
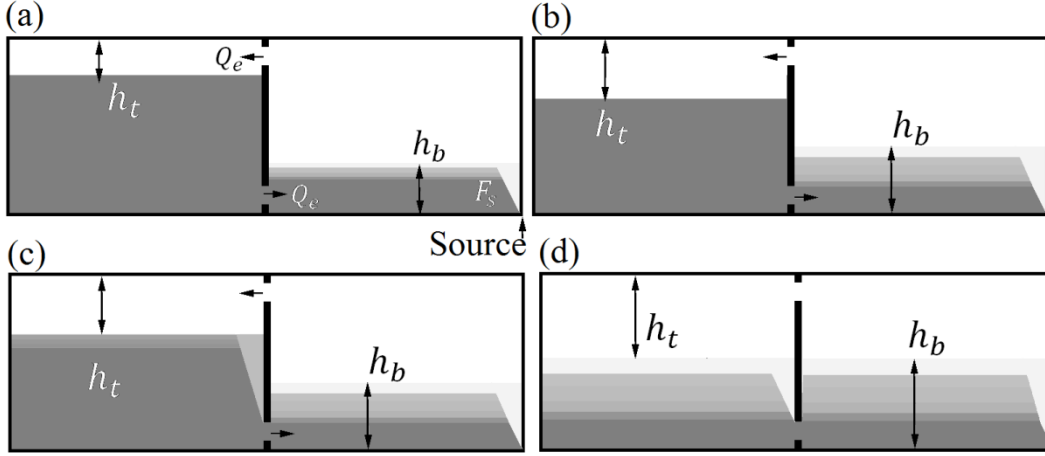

Figure 2. Schematic of the displacement exchange flow with a source, which is located in the bottom right hand corner of the light zone at (a) $t < t_3$ when the stratification due to the source lies strictly above the top of the bottom vent in the light zone, (b) $t = t_3$, (c) $t_3 < t < t_s$ when a plume rises through the lower layer of the dense zone (d) $t = t_s$ when the source is turned off. Here t_3 is the time required for the first front to reach to the top of the bottom vent and t_s is the time during which the source is switched on.

It should be noted that when $N_b/N_t = 0$ or ∞, resulting in exchange flow associated with a single doorway (mixing ventilation), a two-layer exchange flow is established, resulting in a buoyant plume that rises through the dense zone and a horizontal gravity current that propagates through the light zone. Over time, a stratified ambient develops in the dense zone, and depending on the geometrical parameters discussed in [10, 11] the light zone will include two distinct layers with a possible intermediate stratified layer. Conversely in the displacement ventilation flow that is the topic of this paper, by opening the top and bottom vents simultaneously unidirectional flow of opposite sign is observed through the bottom and the top vents. This in turn, evolves into horizontal gravity currents that run along the floor and ceiling of the space. Therefore, unlike in the mixing ventilation scenario, we anticipate a two-layer stratification in each zone with a sharp density jump from one layer to the other. Upon reflection from end walls, floor and ceiling gravity currents yield internal bores (Figure 1c). In the present

study, we refer to the gravity currents and resulting internal bores as horizontal currents.

As with mixing ventilation, Q_e decreases once the internal bores reach the doorway. We denote this time as $t_{2,j}$ where $j = b$ or t indicating the bottom and top flow, respectively. (By contrast, $t_{1,j}$ corresponds to the time required for the horizontal current to reach to the end walls) However, unlike in mixing ventilation, Q_e now tends to zero in a finite time t_E, rather than an infinite time. For times larger than $t_{2,j}$ a horizontal interface develops in each zone; in the light zone a layer with depth h_b moves upward and, meanwhile, a layer with depth h_t travels downward in the dense zone (Figure 1d). For $t > t_E$, the interface elevations do not change as a function of time.

Due to numerous differences between the two modes of exchange flow described above, displacement ventilation merits its own investigation, all the more so because, as we shall see, Q_e is now typically larger than for the cases examined in [10, 11]. Therefore, if the purpose is to redistribute buoyancy from an attached solarium as quickly as possible, the architectural design associated with only a common doorway is inferior to that of Figure 1, where there are both top and bottom vents. We extend the displacement ventilation analysis further in an architecturally meaningful way by including an isolated source of buoyancy in the light zone as shown in Figure 2. Over the time, t_s, that it is active or "switched on", the source thereby continually increases the thermal energy within the building envelope in addition to the energy that is transferred as a result of the exchange flow depicted in Figure 1. Thus, the source introduces additional dynamics, which are superimposed on top of those associated with a simple two-zone exchange flow.

The rest of the manuscript is organized as follows: the mathematical model is developed in Section 2. A discussion of theoretical predictions is also included in therein. In Section 3, the experimental setup and procedure is explained. In Section 4, we compare theoretical and experimental results to understand the nature of displacement flow and assess the validity of the model

equations from Section 2. Conclusions and future considerations are drawn in Section 5.

2 Theory

We seek a theoretical framework to describe the evolution of density and buoyancy in each zone with respect to time and space. As we will see later, the dynamics of each zone are highly coupled to one another.

Only vertical stratification is considered in this study. It is assumed that there are no fabric heat losses or gains through the ceiling or floor and that the building is well insulated. Following our previous analysis [10, 11], the system is assumed to be incompressible and Boussinesq and the pressure distribution hydrostatic. For analytical convenience, the plume is assumed to be switched on at $t = t_{2,b}$, not $t = 0$, the instant when the bottom and top vents are simultaneously opened. Such an assumption has only a minor impact on the dynamics of the displacement exchange flow because during $0 \leq t \leq t_{2,b}$, the buoyancy added to the system from the source is insignificant compared to that gained (lost) in the light (dense) zone by the exchange flow. Finally, any entrainment or detrainment into or out of horizontal currents is ignored.

2.1 Ventilation flow with no source of buoyancy

We start by analyzing $F_s=0$. For purposes of analytical efficacy the problem is divided into three complementary parts: i) two counterpart exchange flows, both of which are unidirectional and which arise due to a difference of hydrostatic pressure between the adjacent building zones, ii) horizontal currents comprising the bottom and top gravity currents and associated internal bores and iii) the vertical motion of the interface in each zone.

Four scenarios in terms of the values for h_b and h_t at $t = t_2$ are possible depending on the bottom and top effective areas and relative size of the two zones. Here we only focus on the scenario where both $\frac{h_{2,b}}{(h+D)} > 1$ and $\frac{h_{2,t}}{(h+D)} > 1$, which is the most architecturally relevant. It can be proved that this is not a limiting consideration [23].

2.1.1 Exchange flow rate Q_e and interface height

By simultaneously opening the top and bottom vents, two oppositely-directed exchange flows, whose magnitudes are equal by volume balance, are established. The respective conservation of volume equations read as

$$Q_e = u_b a_b = u_t a_t \tag{1}$$

Here u_b (u_t) is the velocity thorough the bottom (top) vent(s) whose respective total areas are a_b (a_t). We assume a circular vent geometry so that a_b and a_t are given by $N_b \frac{\pi}{4} D^2$ and $N_t \frac{\pi}{4} D^2$, respectively.

To determine Q_e, some estimate of the pressure distribution in each zone is needed for which purpose we suppose that the (horizontally uniform) pressure along the ceiling of the dense and light zone is, respectively, $p_{c,t}$ and $p_{0,t}$. A straightforward application of Bernoulli's equation shows that

$$Q_e = \sqrt{2\frac{\Delta p_b}{\rho_0}} a_b = \sqrt{2\frac{\Delta p_t}{\rho_0}} a_t \tag{2}$$

in which the pressure difference Δp_t is given by $\Delta p_t = p_{0,t} - p_{c,t}$. Also, by hydrostatic balance,

$$\Delta p_b = (\rho_0 - \rho_c)(H - h_b - h_t)g - \Delta p_t \tag{3}$$

Substituting (2) and (3) into (1), we find that

$$Q_e = A^* \sqrt{g'(H - h_b - h_t)} \tag{4}$$

where $g' = g \frac{\rho_0 - \rho_c}{\rho_{00}}$ is the reduced gravity with ρ_{00} as a reference density, e.g. the density of the cold zone, and A^* is the effective vent area and is defined by

$$A^* = \frac{a_b a_t}{\sqrt{\frac{1}{2}(a_b^2 + a_t^2)}} \tag{5}$$

This result neglects any dissipation via entrance and exit effects. Incorporating these losses yields an equation equivalent to (1.4) of Kaye and Hunt [24], i.e.

$$A^* = \frac{a_b a_t}{\sqrt{\frac{1}{2}\left(\left(\frac{a_b}{c_b}\right)^2 + \left(\frac{a_t}{c_t}\right)^2\right)}} \tag{6}$$

where c_b and c_t are, respectively, the discharge coefficients associated with the bottom and top vents. Consistent with [24], we assume $c_b = c_t = 0.6$.

Equation (4) is similar to (2.4) of Linden et al. [7], which specifies the exchange flow rate between an interior and exterior. A key difference is that here Q_e depends on two interface heights i.e. h_b and h_t. The time evolution of these can be connected by applying conservation of volume, according to which

$$Q_e = (L - \ell)W\frac{dh_b}{dt} = \ell W\frac{dh_t}{dt} \tag{7}$$

Equations (4) and (7) therefore constitute a coupled pair of autonomous ordinary differential equations, whose solution requires the specification of a pair of starting conditions i.e.

$$h_b = h_{2,b} \text{ at } t = t_{2,b} \tag{8a}$$

$$h_t = h_{2,t} \text{ at } t = t_{2,t} \tag{8b}$$

Note also that conservation of volume gives the relationship between h_b and h_t:

$$h_t = \frac{L - \ell}{\ell}h_b \tag{9}$$

We employ (8), as starting conditions, to solve (7). Upon applying (4), integrating and simplifying, it can be shown that

$$\frac{h_b}{H} = \left[1 - \left(\sqrt{\left(1 - \frac{L}{\ell}\frac{h_{2,b}}{H}\right)} - \frac{(t - t_{2,b})}{\frac{T_E \ell}{L}}\right)^2\right]\frac{\ell}{L} \tag{10}$$

where T_E is given by

$$T_E = \sqrt{\frac{H}{g'}}\left(\frac{2(L - \ell)W}{A^*}\right) \tag{11}$$

In physical terms, T_E is similar to the draining time defined by (2.8) of Linden et al. [7] with the difference that here we are concerned with the flow between two adjacent building zones. In our case, therefore, T_E does not correspond to the time required to reach steady state. The relevant time-scale is instead t_E, which is defined as

$$\frac{t_E}{T_E} = \frac{L}{\ell}\left(\left[\sqrt{\left(1 - \frac{L}{\ell}\frac{h_{2,b}}{H}\right)}\right] + \frac{t_{2,b}}{\frac{T_E \ell}{L}}\right) \tag{12}$$

Note that when $t = t_E$, Q_e, dh_b/dt and dh_t/dt are all zero. Moreover, using (10) it can be shown that $h_b/H = \ell/L$ when $t = t_E$. By increasing ℓ/L or decreasing the effective area, A^*, t_E increases and, therefore, it takes more time for the interfaces to reach their terminal elevations. t_E is the time-scale with which we choose to non-dimenionalize time $\tau = t/t_E$, unless otherwise stated.

2.1.2 Theory for horizontal flows

1- Gravity current formulation:

We use the Benjamin equation [25] for the front speed, u_1, in terms of the front height, h_1

$$\frac{u_1^2}{g'H} = \frac{h_1(H - h_1)(2H - h_1)}{H^2(H + h_1)} \tag{13}$$

along with the equation for mass conservation, which leads to the following expression for the initial volumetric exchange rate

$$Q_e = u_1 h_1 W \tag{14}$$

2- Internal bore formulation:

We use the Klemp et al-type approach [26]

$$\frac{u_2^2}{g'H} = \frac{h_1^2(H - h_1)(2H - h_1 - h_2)}{H^2(Hh_1 + Hh_2 + h_1^2 - 3h_1h_2)} \tag{15}$$

which establishes the connection between the bore speed, u_b, and the bore height, h_b. Equation (15) is coupled to a mass conservation equation, here expressed as

$$Q_e = u_2(h_2 - h_1)W \tag{16}$$

Assuming constant velocity for the horizontal currents, we have

$$t_{2,b} = (L - \ell)\left(\frac{1}{u_{1,b}} + \frac{1}{u_{2,b}}\right) \tag{17a}$$

$$t_{2,t} = \ell\left(\frac{1}{u_{1,t}} + \frac{1}{u_{2,t}}\right) \tag{17b}$$

Equations (17) show that for $\ell/L < 1/2$ ($>1/2$) we have $t_{2,b} > t_{2,t}$ ($t_{2,b} < t_{2,t}$). Obviously, when the two zones are equal in size $t_{2,b} = t_{2,t} \equiv t_2$.

2.1.3 Buoyancy

We define the non-dimensional total buoyancy in a specified control volume (c.v.) as

$$b_{c.v.} = -\frac{1}{g'HL} \iint g \frac{\rho_{c.v.} - \rho_0}{\rho_0} \, dz dx \qquad (18)$$

The total initial buoyancy of the system is

$$b_{tot}(0) = \left(1 - \frac{\ell}{L}\right) \qquad (19)$$

2.2 Ventilation flow with a source of buoyancy

We now extend our analysis to take into account the impact of an isolated source, which is turned on at $t = t_2$ for a time interval $t_s \gg t_2$. The source consists of an ideal line plume distributed uniformly along the width of the light zone with a buoyancy flux and area of F_s and A_s, respectively.

We assume the stratification, which is described by a filling-box process [19], is confined to the region below the interface, i.e. $0 < z < h_b$. Above this region the plume density is larger than the light zone fluid and the buoyancy force is downward. Although the plume momentum flux is larger than 0, which may allow the plume to ascend above the interface, consistent with [27], we ignore such an overshoot. The vertical expanse of the control volume into which the plume ascends increases with time, i.e. $\frac{dh_b}{dt} > 0$. The plume/ambient interaction therefore depends on the exchange flow rate and interface height, which is in turn influenced by the filling-box process and stratification associated with plume. Accordingly dense fluid of density ρ_0 is separated from fluid originating from the plume by a horizontal "first front" of elevation z_{ff} that descends over time.

Because the bottom vent is above the source origin, the advecting first front is able to reach the top of the bottom vent(s) in finite time, say, t_3. In the present circumstance, any layer advected below $z = h + D$ will flow into the dense zone and form N_b separate axisymmetric plume(s), as we illustrate schematically in Figure 2. We denote the light and dense zone density below the interface in each zone as $\rho_{a,c}(z,t)$ and $\rho_{a,0}(z,t)$, respectively.

2.2.1 Exchange flow rate Q_e and interface height

Consistent with the above discussion, we assume a hydrostatic pressure distribution, we write

$$\Delta p_b = \rho_c g h_t + \int_{h+\frac{D}{2}}^{H-h_t} \rho_{a,o} g dz - \rho_c g (H - h_b)$$

$$- \int_{h+\frac{D}{2}}^{h_b} \rho_{a,c} g dz - \Delta p_t \tag{20}$$

as the pressure difference between two points immediately to the left and right of the bottom vent. Upon applying conservation of volume, it can be shown that the exchange flow rate is given by

$$Q_e = A^* \sqrt{g'(H - h_b - h_t) + \int_{h+\frac{D}{2}}^{H-h_t} \Delta_{a,o} dz - \int_{h+\frac{D}{2}}^{h_b} \Delta_{a,c} dz} \tag{21}$$

Here A^* is defined by (6) and $\Delta_{a,o}$ and $\Delta_{a,c}$ are the characteristic reduced gravities of the dense and light zones, respectively, and are defined as

$$\Delta_{a,0} = g \frac{\rho_{a,0} - \rho_0}{\rho_0} \leq 0 \tag{22a}$$

$$\Delta_{a,c} = g \frac{\rho_{a,c} - \rho_0}{\rho_0} \leq 0 \tag{22b}$$

When the dense and light zone stratification is due to the filling-box process, it is impossible to solve (7) and (8) analytically. Rather, a numerical solution is sought.

2.2.2 Buoyancy

Due to the source of buoyancy, the total buoyancy is now not conserved. To wit

$$b = \left(1 - \frac{\ell}{L}\right) + b_s \tag{23}$$

where b_s, the buoyancy added to the system by the source at any instant, is

$$b_s = \frac{F_s(t - t_2)}{g'WHL} \tag{24}$$

The dense and light zone buoyancy can be written as

$$b_0 = -\left(\int_{h+\frac{D}{2}}^{H-h_t} \frac{\Delta_{a,o}}{g'} \frac{dz}{H} - \left(\frac{h_t}{H}\right)\right)\left(\frac{\ell}{L}\right) \tag{25a}$$

$$b_c = -\left(\int_{h+\frac{D}{2}}^{h_b} \frac{\Delta_{a,c}}{g'} \frac{dz}{H} - \left(1 - \frac{h_b}{H}\right)\right)\left(1 - \frac{\ell}{L}\right) \tag{25b}$$

respectively. Applying (9), it can therefore be shown that

$$b_s = -\left[\int_{h+\frac{D}{2}}^{H-h_t} \frac{\Delta_{a,o}}{g'} \frac{dz}{H}\right]\left(\frac{\ell}{L}\right) - \left[\int_{h+\frac{D}{2}}^{h_b} \frac{\Delta_{a,c}}{g'} \frac{dz}{H}\right]\left(1 - \frac{\ell}{L}\right) \tag{26}$$

and, by extension,

$$Q_e = A^* \sqrt{g'(H - h_b - h_t) - \frac{g'HL}{\ell} b_s + \frac{L}{\ell}\int_{h+\frac{D}{2}}^{h_b} \Delta_{a,c} dz} \tag{27}$$

Equation (27) expresses the exchange flow rate as a function of the buoyancy added to the system.

The buoyancy in each zone can be decomposed into two components at any moment in time: that associated with the displacement ventilation illustrated schematically in Figure 1 and that due to the buoyant plume rising from the source. Note that, however, for $t < t_3$ the buoyancy increases in the dense zone only due to the displacement mechanism

We now define Π_s, the source strength, as

$$\Pi_s = \frac{F_s t_s}{g'HW(L - \ell)} \geq 0 \tag{28}$$

Equation (23) indicates that Π_s is the ratio of the buoyancy added by the source over time t_s and the total buoyancy of the system at $t = 0$.

Two flow regimes can be discerned on the basis the magnitude of Π_s: 1) a ventilation-dominated regime with $0 < \Pi_s \leq 1$ and 2) a source-dominated regime with $\Pi_s > 1$. In this study, particular attention is focused on the former. Note that, $\Pi_s = 0$ is a special limiting case where there is no buoyancy source in the system. For the $\Pi_s > 0$, one can further divide the ventilation dominated regime into regions where the influence of the source is weak, moderate and strong. Somewhat arbitrarily, we assign these regions to Π_s values in the respective ranges $0 < \Pi_s < 0.1$, $0.1 \leq \Pi_s \leq 0.5$ and $0.5 < \Pi_s \leq 1$.

2.2.3 Plume/ambient interaction

2.2.3.1- **Stratification in the light zone**:

The interface height in the light zone, h_b, is simultaneously a function of Q_e and the stratification in each zone. In order to determine the details of this stratification, we solve the equations describing the evolution of the flux of volume, Q, momentum M, and buoyancy F within the ascending plume. These read [18]

$$\frac{dQ}{dz} = \sqrt{2}\alpha \frac{M}{Q} \tag{29-a}$$

$$\frac{dM}{dz} = \sqrt{\frac{1+\lambda^2}{2}} \frac{FQ}{M} \tag{29-b}$$

$$\frac{dF}{dz} = Q \frac{\partial \Delta_{a,0}}{\partial z} \tag{29-c}$$

, respectively, where λ is an empirical constant equal to 1.16 [36] and the entrainment coefficient α=0.14. The physical meaning of λ is analogous to Schmidt number which characterizes the ratio of momentum to mass diffusivity (transport). Whereas the choice of λ or α has a mild impact on the particulars of the density stratification, its numerical value is immaterial insofar as the total buoyancy exchanged between the two zones. Conversely, the dense zone ambient stratification evolves according to an advection equation that reads [19]

$$\frac{\partial \Delta_{a,0}}{\partial t} = U \frac{\partial \Delta_{a,0}}{\partial z} \tag{30}$$

subject to $Q = M = 0, F = F_s$ at $z = 0$ as the boundary conditions. Note that here the advection velocity of individual layers within the light zone, U, is defined as

$$U = \frac{Q_e - Q}{L - \ell} \tag{31}$$

2.2.3.2- **Stratification in the dense zone**:

The plume(s) that rise through the dense zone issue from circular vents along the bottom of the interior wall for $t > t_3$, provided the vent spacing is sufficiently large so that plumes do not directly interact. In this case (29) and (30) should be solved over $0 < z < H - h_t$ with the difference for the continuity equation which should now read as

$$\frac{\partial Q}{\partial z} = 2\alpha_d \sqrt{\pi M} \tag{32}$$

The entrainment coefficient for axisymmetric plumes is $\alpha_d = 0.082$ (Table 2 of [18]). Moreover, the layer advection velocity, U, in case of multiple plumes is given by [28]:

$$U = -\frac{N_b Q}{\ell} \tag{33}$$

Regarding the dense zone source conditions at $z = h + D$ the volume, momentum and buoyancy fluxes are given by their counterpart quantities associated with the advecting layers in the light zone. Germeles numerical scheme is modified and used to solve the plume equations in each building zone [21]. At the heart of his algorithm is the assumption that the plume evolution, when marching forward in time, can be decoupled from the evolution of the ambient stratification. A series of layers with discrete density steps represent the ambient stratification. Hence, the Germeles scheme is sometimes called a "layering" method. In this approach, Runge-Kutta and Euler schemes, respectively, are used for the spatial and temporal discretization. Also note that the source conditions for the dense zone are time-variable but not so for the light zone.
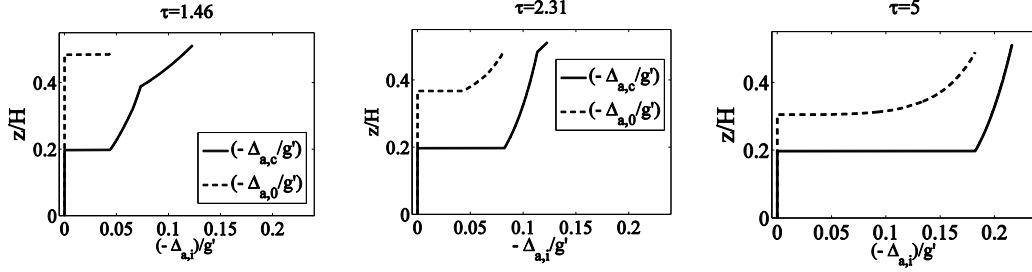
2.3 Model predictions
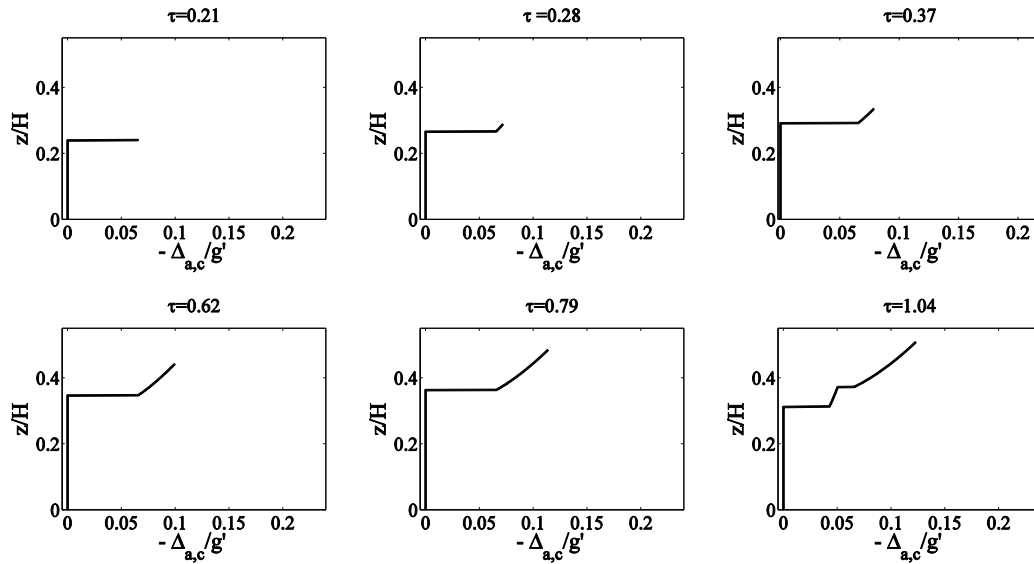
Figure 3. Dimensionless stratification profiles, scaled by $-g'$, with respect to elevation, scaled by H, at different dimensionless times, τ. The solid and dashed curves correspond to the stratification in the light and dense zones, respectively.

Figure 3 shows the spatio-temporal evolution of the density in the light and dense zones. In Figure 3 the ambient stratification is shown only below the interface. Above the interface, there is unmodified light fluid, i.e. $-\Delta_{a,c}/g'=-\Delta_{a,0}/g'=1$ for $h_b/H<z/H<1$ and $1-h_t/H<z/H<1$. In Figure 3, $\Pi_s=0.10$, $A^*/(\frac{\pi}{4}D^2)=1.93$ and $\frac{\ell}{L}=0.5$. The top of the bottom vent(s) extend 20% of the way up the common wall, i.e. $(h+D)/H=0.2$. Also, $t_E=118$ and $\tau_3=\frac{t_3}{t_E}=1.45$. Finally $\tau_2=\frac{t_2}{t_E}=0.20$, which is significantly smaller than the non-dimensional time the source is activated, i.e. $\tau_s=5$.

Figure 3 confirms that the motion of the first front differs in a nontrivial way from that considered in [10, 11 and 14]. Here it follows a non-monotonic trend; up until $\tau=0.787$, all the stratified layers in the light zone, including the first front, move upwards. Thereafter, the time rate of change of h_b is small enough that the layers, which always move downwards relative to the interface, now also move downwards relative to a fixed observer. Such behavior is also reflected by (31); initially $Q<Q_e$ and $U>0$. Due to a progressive drop in the hydrostatic pressure difference between the two zones, however, Q_e decreases so that, eventually, $Q>Q_e$ and $U<0$.

Concerning the light zone stratification, at $\tau=1$, when $U\leq0$, we have $-\Delta_{a,c}/g'=0$ for $0<z/H<0.37$ and $-\Delta_{a,c}/g'>0$ for $0.37<z/H<1$. $-\Delta_{a,c}/g'=0$ corresponds to the dense fluid density; therefore, due to entrainment of this dense fluid, the plume density will become equal to the ambient density at a point below the interface of light zone. At this elevation and, consistent with the approach taken in [10, 11], we assume that the plume spreads in the lateral direction. For the panels with $\tau=1.04$, 1.46 and 2.31 in Figure 3, this elevation is

18

evident as the kink in the solid curve that appears at z/H=0.37, 0.39 and 0.48, respectively. As the filling-box process continues, a progressively larger fraction of the lower layer becomes density-stratified which results in a smaller density within the plume. As a result, the kink disappears in the long time limit as indicated by the stratification profile in the τ=5 panel of Figure 3.

Regarding the dense zone stratification, for $\tau > \tau_3$=1.45, the first front reaches the top of the bottom vents, and there is a flow of stratified ambient fluid into the dense zone that is characterized by N_b =3 vertically rising plumes in Figure 3. In contrast to the light zone the layers in the dense zone move in the downwards direction for all τ ($>\tau_3$).

Figure 4 explores the dependence of τ_3 with Π_s and A^*. As Π_s decreases, τ_3 increases sharply: for weak sources of buoyancy larger times are required for the dense zone to feel the influence of the buoyant source in the adjacent light zone. Note, however, that for very large values of Π_s, τ_3 becomes nearly independent of Π_s. Also shown in Figure 4 is that for larger A^* values, the downward motion of the first front in the light zone begins more rapidly, leading to smaller values for t_3. However, t_E decreases by an even larger fraction so that $\tau_3 = t_3/t_E$ increases.
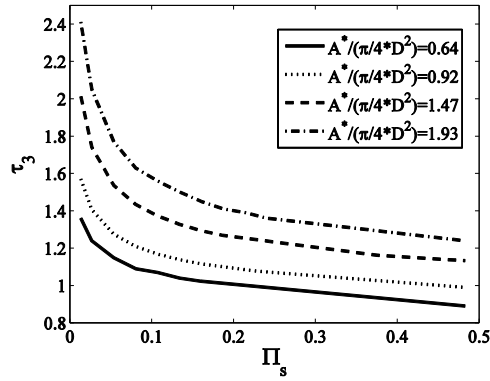

Figure 4. Variation of $\tau_3 = t_3/t_E$ with respect to Π_s for various $A^*/(\frac{\pi}{4}D^2)$.

Figure 5 shows the buoyancy scaled by $b_{tot}(0)$, given by (19), versus τ for various values of Π_s. Panel a indicates that the buoyancy in the light zone first decreases with time and then increases so that $db_c/d\tau$ =0 at a time close to τ =1. In particular, for Π_s =0.015, 0.075, 0.150 and 0.225, $b_c/b_{tot}(0)$ =0.5019, 0.5061, 0.5128 and 0.5197 as the local minimums at τ_{min} =1.01, 1.01, 1.00 and

1.00, respectively. The minimum occurs because by opening vents, light fluid is replaced by an equal volume of dense fluid, which results in a decrease of buoyancy for $0<\tau<\tau_{min}$. At τ_{min}, Q_e has decreased to the point where negligible buoyancy is lost due to ventilation. As such, the buoyancy delivered by the source becomes increasingly more significant, so that it outweighs the buoyancy lost through the upper vent(s). Note, moreover, the slight change of slope that occurs when $\tau = \tau_3 =$ 2.06, 1.47, 1.29 and 1.21. When there is a buoyancy source, b_0 is not the mirror image of b_c in contrast to the mixing ventilation case [11]. For $\tau > \tau_3$, b_0 increases because the first front has now reached the top of the bottom vent, providing a further means by which buoyant fluid may enter the dense zone.
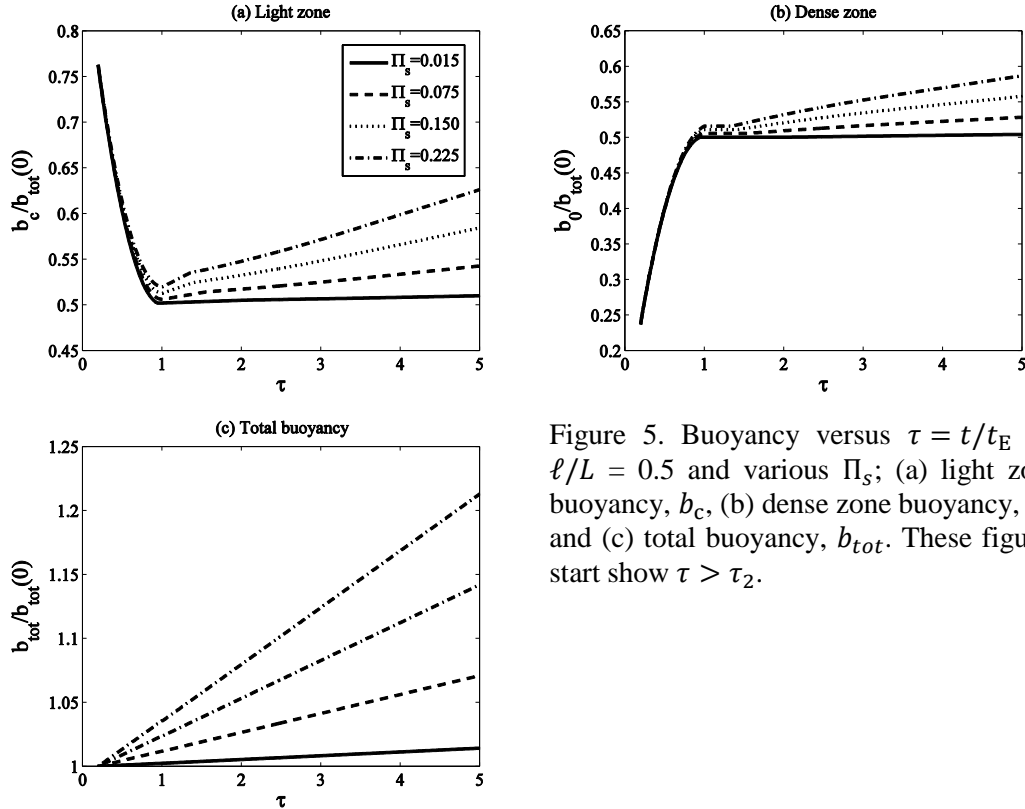

Figure 5. Buoyancy versus $\tau = t/t_E$ for $\ell/L = 0.5$ and various Π_s; (a) light zone buoyancy, b_c, (b) dense zone buoyancy, b_0, and (c) total buoyancy, b_{tot}. These figures start show $\tau > \tau_2$.

Note finally that the above analysis presumes the source to be ideal so that the source volume and momentum fluxes are zero. This assumption is reasonable from the point of view of modelling solar gains in equator facing zone(s), but it is difficult to reproduce experimentally using a salt-bath system. For this reason, it is necessary to extend the above model to include the case of a (weak) non-ideal source. In a real building, whose geometry is obviously fixed, a non-ideal source acts to increase the interior pressure, because the total depth in each zone cannot

20

increase further. Even so, provided $\Pi_s \ll 1$, one can assume the density deviation of any point from its initial value is small and that the system remains Boussinesq.

3 Similitude laboratory experiments

Following a long line of earlier studies (as summarized in e.g.[22]), we ran similitude experiments using water as the working fluid which makes it possible to achieve architecturally relevant Re number at small spatial scales. The experiments were conducted in a 227.5 cm long, 25.0 cm wide and 34.5 cm deep glass tank. A 25.0 cm wide by 57.5 cm tall perforated divider 1.5 cm in thickness was used to subdivide the tank. This divider was placed inside the tank to form a fixed $\ell =72.5$ cm long space that served as the dense zone. A second divider was also used to limit the tank length to $L=149$ cm. In this way, the entire flow field could easily be captured using a single camera. Dividers were held in place using putty and silicon glue, which eliminated any leakage of fluid.

Density differences were produced by addition of sodium chloride and were measured using an Antor Paar DMA 4500 densitometer with a precision of ±0.00005 gcm^{-3}. Fresh ($\rho_c \simeq 0.9984$ gcm^{-3}) and saline ($\rho_0 \simeq 1.0400$ gcm^{-3}) water served as the light and dense fluids, respectively, and were replenished after each experiment. Whereas for most experiments $g' =0.40\pm0.02$ ms^{-2}, a limited number of experiments using $0.18<g'<0.49$ ms^{-2} were also conducted to ensure that viscous effects played only a second-order role. More formally, a Reynolds number was defined as

$$\text{Re} = \frac{\sqrt{g_0' H^3}}{2\nu_{water}} \tag{34}$$

Experiments we conducted in the range $1\times10^4<\text{Re}<3\times10^4$ so that, as with the analogue flow in real buildings, transport is overwhelmingly due to turbulent, rather than molecular, effects [29]. Red food dye was added to the either the dense or light fluid for visualization purposes.

The tank was filled with fresh water to a depth of $H =21\pm0.5$ cm so that the distance ($h=1.5$ cm) from the top vent to the free surface matched the distance from the bottom vent to the bottom of the tank. The experiments were carried out for the range of $1\leq N_b \leq3$ and $1\leq N_t \leq3$, where N_b and N_t are the number of

open vents, with diameter 2.54 cm, along the bottom and top of the dividing wall, respectively. At the beginning of a particular experiment, special care was taken to remove the stoppers simultaneously so as to avoid a two-layer exchange flow through any one vent.

A plume nozzle, which spanned the tank width, was placed at the bottom of the tank along the end wall of the light zone and was supplied by a constant-head pump (Masterflex L/S peristaltic device). The pump supplied fresh fluid at a constant rate over the course of each experiment. Values of Q_s and t_s in the respective ranges of $1 < Q_s < 6$ mls^{-1} and $600 < t_s < 5400$ s were used, which resulted in source strength values in the range $0.01 \leq \Pi_s \leq 0.28$ according to which the flow was always ventilation-dominated. Larger values of Π_s were avoided because they either entail (i) large Q_s so that the plume is in actuality a buoyant jet, (ii) large $\rho_0 - \rho_c$ so that the system is non-Boussinesq and/or (iii) large t_s over which there is an appreciable change of elevation of the free surface.

The plume nozzle was designed using SolidWorks and was manufactured by Rapid Prototyping. Figure 6 shows a schematic of the nozzle which, as much as possible, was designed so as to produce a flow that was uniform along its length. The nozzle was fixed to the front and back face of the tank with special brackets manufactured using a water jet cutter. The plume nozzle was always positioned at $z = 0$. We use a constant head pump, but the flow rate is kept as small as reasonably possible so that the flow is buoyancy-driven everywhere except very close to the plume source. The jet-length, L_j is defined as the height over which the flow is dominated by the momentum flux and has the characteristics of a jet rather than a plume. Hunt et al. [34] give the following equation to estimate the jet length in an environment of depth H:

$$\frac{L_j}{H} = \frac{M_s^{3/4}}{H F_s^{1/2}} \tag{35}$$

where M_s is the source momentum flux and is scaled as $Q_s^2/t \times W$ in our experiments. Therefore, for a typical experiment $L_j/H \cong 5 \times 10^{-4}$ which implies that the jet-length is very small compared to the height of the tank and it is expected for the source to behave like a plume after a very small distance.
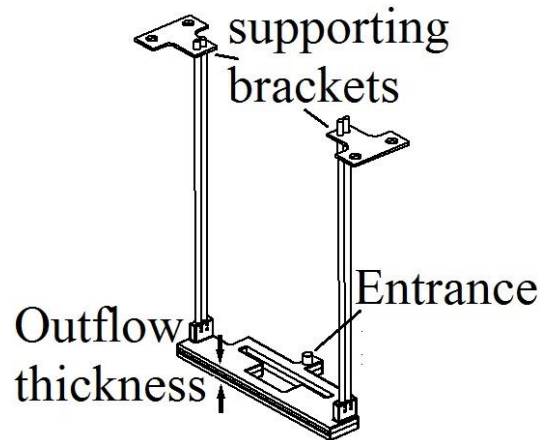
Figure 6. Schematic of the nozzle.

By employing a 12 in by 72 in light-sheet (Electric Vinyl, PNP1724), the tank was uniformly backlit. Images were recorded using a LaVision Imager E-lite camera with 35 mm Nikon AF Nikon lens. The linear gain of the CCD camera and direct recording to digital format reduced noise and simplified later analysis. A MATLAB algorithm was developed and used for analysis of the experimental data in order to measure the velocity and depth of the horizontal flows as well as the time rate of change of interface height in both zones. By identifying the location of a sudden change of pixel intensity, we could straightforwardly the front speeds of either a gravity current or bore. A similar methodology was used to estimate the interface elevations in the dense and light zones. Note, however, that the depths of the horizontal currents varied along their length achieving, in the case of the gravity current, a maximum at the raised head and a minimum between the head and the tail. To avoid such complications in the present analysis we only report interface heights for $\tau > \tau_2$.

We used a conductivity probe (Precision and Measurement Engineering, MSCTI) to measure the terminal ambient stratification in the dense zone. For calibration of the probe, we gathered five samples from the ambient medium and used these to find the linear relationship between the voltage measured by the probe and the fluid density. The probe was mounted on a vertical traverse (Velmex, X-Slide), whose translational speed was typically 5 mm/s, which was found to be small enough not to disturb the dense or light zone ambient fluid.

4 Results and discussion

Figure 7 shows the variation of interface height in the light and dense zones as a function of time for various source buoyancy fluxes and effective vent areas. As expected, the rate of change of h_b and h_t is more substantial for $\tau \leq$ 0.6. Conversely when $0.6 \leq \tau < 1$, the rate of increase is comparatively slow and for $\tau > 1$, it is identically zero. The eventual time independence of h_b and h_t is not only predicted by theory; it is also strongly suggested by the laboratory measurements where, in general, no distinguishable variation of interface height is observed for $\tau > 1$. Moreover, for larger values of the effective vent area, the depth of the internal bore at $\tau = \tau_2$ is larger, so that h_b or h_t start off with a larger value. Error bars, are based on the results of repeat experiments, conducted for select combinations of N_b, N_t, F_s and t_s [31].
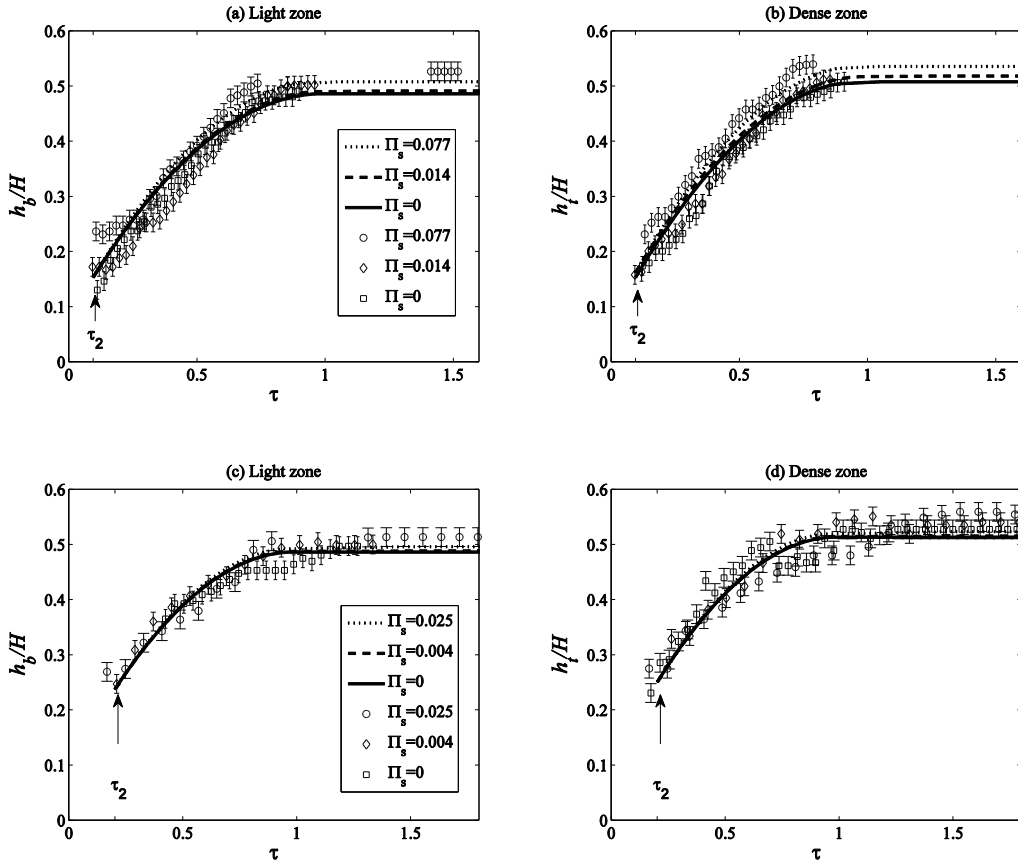

Figure 7. Interface height in the light (h_b/H) and dense (h_t/H) zones versus non-dimensional time τ. $A^*/(\frac{\pi}{4}D^2) = 0.64$ for panels (a) and (b), $A^*/(\frac{\pi}{4}D^2) = 1.93$ for panels (c) and (d).

From the different panels of Figure 7, it can be shown that for $\tau > \tau_2$ and time-invariant source conditions, the interface height follows a universal trend for all values of $A^*/(\frac{\pi}{4}D^2)$, provided time is scaled by t_E. This observation affirms the physical importance of t_E, defined by (12), in displacement ventilation flows of the type illustrated schematically in Figure 2.

Figure 8 shows the variation of $t_E/t_{E,max}$ as a function of $A^*/(\frac{\pi}{4}D^2)$ for the same value of Π_s. (Similar results are obtained for other values of the source strength). Here, $t_{E,max} =361$ s is the maximum ending time and, for this set of experiments, corresponds to the minimum value of A^*. As noted in connection with Figure 7, the vent size has a significant effect on the starting value of h_b and h_t. A^* also determines how quickly the light zone exchanges fluid with the dense zone. Hence, by increasing A^* in Figure 8, $t_E/t_{E,max}$ decreases.
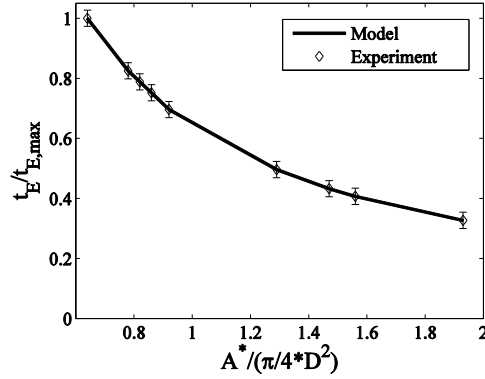

Figure 8. Variation of the ending time, $t_E/t_{E,max}$, as a function of effective area, $\frac{A^*}{\frac{\pi}{4}D^2}$.

As for the light and dense zone stratification, there exists an extensive volume of experimental data. Hence, only select experiments are considered in detail. The final stratification is measured with superscript f. Figures 8 to 11 show the comparison between the experimental and theoretical results for both the light and dense zones. In contrast to Figures 3 and 4, the stratification is now shown as a function of z/H over the entire depth of the control volume. Consistent with Figures 3 and 4, however, τ_s is set to be large enough so that there develops a non-trivial stratification in the light zone.
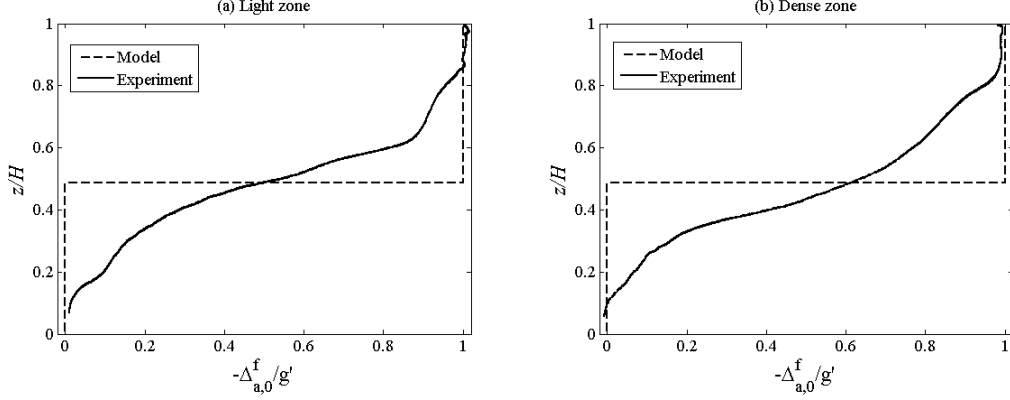
Figure 9. Experimental and theoretical stratification profile in the (a) light and (b) dense zone as a function of z/H for $\Pi_s=0$ and $A^*/(\frac{\pi}{4}D^2)=1.93$. Representative error bar are shown in panel a.

In comparing theory and experiment, we must consider the role of Kelvin-Helmholtz instabilities [32]. Such instabilities result in interfacial mixing which in turn causes a smearing of the sharp interface predicted, for example, in Figure 9. Thus even in the absence of a source of buoyancy there is in the experimental data a non-trivial stratification of density in each zone that is attributed to the mixing associated simply with the propagation of the horizontal currents. This mixing is not accounted for by our equations because, to our knowledge, no analytical model is able to describe such mixing in a straightforward manner.

The ratio of ratio of the diffusion and filling time scales, as suggested by Kaye et al. [6], for small-scale experiments is very large. Hence diffusion plays only a minor role and thereby a relatively thin interface is anticipated. "This suggests that the major effect relates to interfacial mixing that occurs for $t < t_2$. Unfortunately, as noted by Borden and Meiburg [33] "there is no good analytical method" for estimating the thickness of the shear layer associated with gravity current flow. So our ability to make specific quantitative comments here is limited.
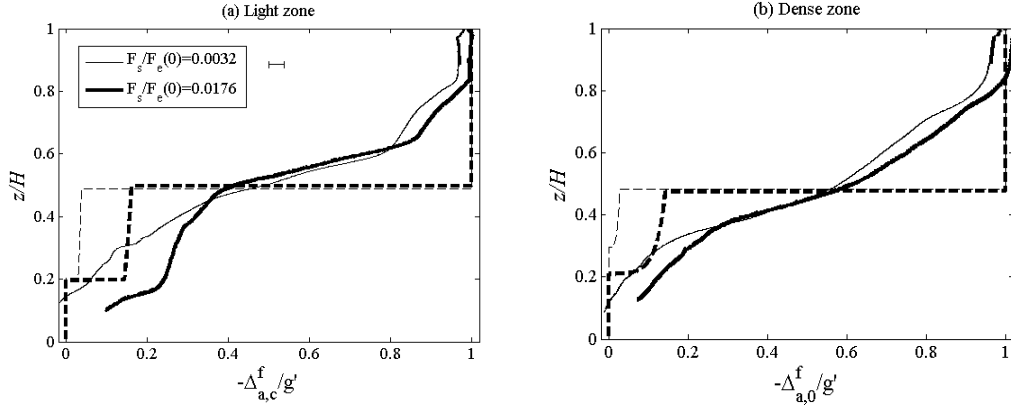
Figure 10. Experimental and theoretical stratification profiles in the (a) light and (b) dense zones as a function of z/H for two different values of $F_s/F_e(0)$ with $F_e(0) = g'Q_e(0)$. $A^*/(\frac{\pi}{4}D^2)$=1.93 and τ_s =5. Theoretical and experimental data are shown by the dashed and solid lines, respectively. A representative error bar is indicated in panel a.

Figure 10 makes apparent the influence of the source buoyancy flux, i.e. $F_s/F_e(0)$, where $F_e(0) = g'Q_e(0)$ is the buoyancy flux associated with the exchange flow at $t = 0$. For larger values of the source buoyancy flux, sharper and greater extent of stratification is shown in both the theoretical and experimental data. Also z/H =0.2, which approximately corresponds to the top of the bottom vent, is the height at which stratified ambient fluid flows from the dense zone into the light zone. Hence, no stratification is observed in the theoretical data for $0 < z/H < 0.2$ in Figure 10.
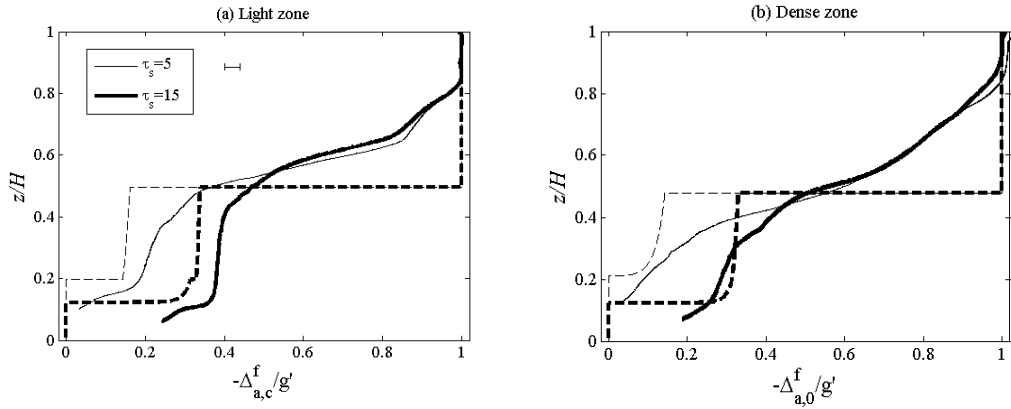

Figure 11. Experimental and theoretical stratification profiles in the (a) light and (b) dense zones as a function of z/H for two different values of τ_s. $A^*/(\frac{\pi}{4}D^2)$=1.93 and $F_s/F_e(0)$ =0.0176.

The influence of τ_s is characterized by Figure 11. Not surprisingly, if the source is active over longer times, the stratification evolves to a greater extent in each zone. Also, for larger values of τ_s, there is greater opportunity for the entrainment of ambient fluid by the plume and, as a result, the stratification below

the interface is predicted to be sharper. In both the theoretical and experimental data, a sharper stratification below the interface is evident for large τ_s.
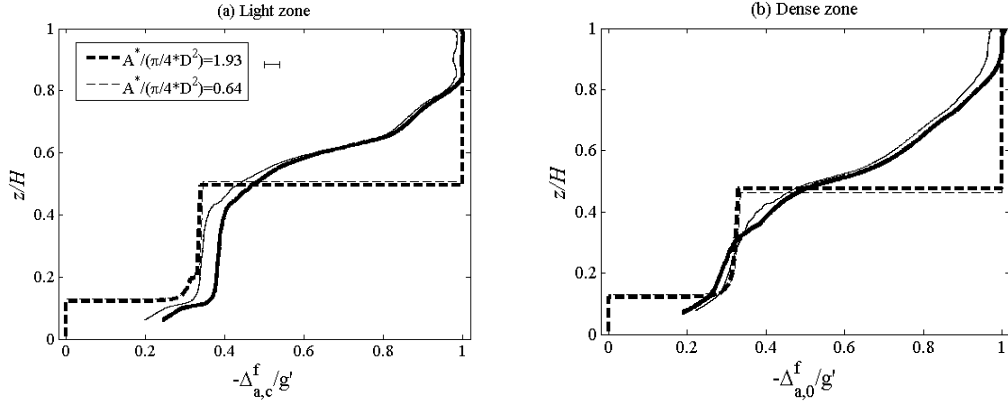

Figure 12. Experimental and theoretical stratification profiles in the (a) light and (b) dense zones as a function of z/H for two different values of $A^*/(\frac{\pi}{4}D^2)$ and Π_s=0.28.

Figure 12 shows the impact of the number of open vents on the stratification profiles in both zones. Clearly, A^* plays a minor role in the final stratification in either zone, a feature that is apparent from both the theoretical and the experimental data.

The analytical model ignores interfacial mixing and the stratification caused by the source is confined to the region below the interface, because the plume buoyancy flux falls to zero for h_b or h_t. Hence, better agreement between model and experiments in Figures 9 to 11 is observed for $z < h_b$ and $z < h_t$.
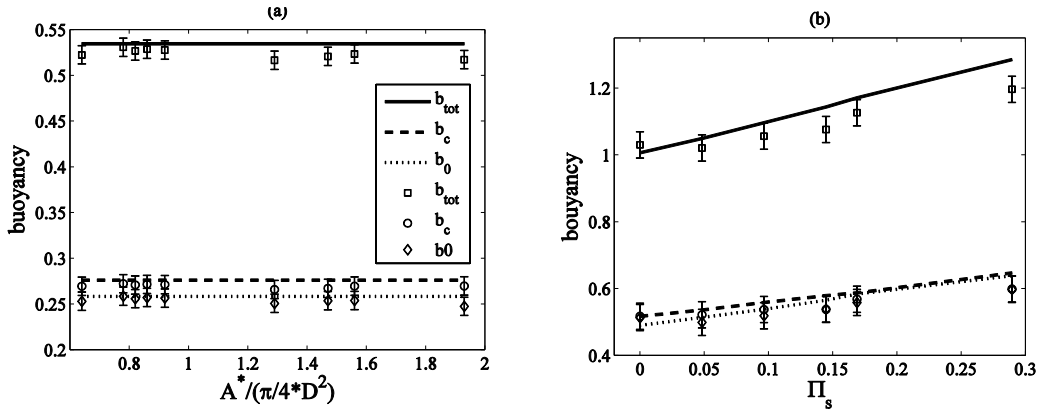

Figure 13. Total, light and dense zone buoyancy, i.e. b_{tot}, b_c and b_0, respectively, as functions of (a) $A^*/(\frac{\pi}{4}D^2)$ for $\Pi_s = 0.0483$ and (b) Π_s for $A^*/(\frac{\pi}{4}D^2)$ =1.93. The lines and markers correspond to analytical and experimental data, respectively.

Figure 13a shows the buoyancy of either zone plotted against $A^*/(\frac{\pi}{4}D^2)$ for Π_s =0.0483. Clearly, the effective area is not expected to alter the final buoyancy provided $\tau_s > \tau_3$ and this prediction is in very good agreement with our

28

laboratory measurements. We also carried out a further set of experiments with $A^*/(\frac{\pi}{4}D^2) = 1.93$ and different values of Π_s as shown in panel (b) of Figure 13. By increasing Π_s, the buoyancy, b_s, added by the source also increases. Therefore in Figure 13b, the buoyancy increases as a monotone function of the independent variable. A similar trend is expected for other values of $A^*/(\frac{\pi}{4}D^2)$. As Figure 13 makes clear, despite the fact that the point-by-point agreement between the solid and dashed curves of Figures 9 to 11 is sometimes lacking, the predicted final buoyancy may still agree well with laboratory measurements.

5 Conclusions

The exchange flow between two adjacent confined zones of slightly different initial density, first developed by Nabi and Flynn [10-11], is extended to cases where there are top and bottom vents, which are opened simultaneously. Two scenarios are considered: the ventilation problem in the absence or presence of a source of buoyancy. An analytical model is derived and similitude laboratory experiments are carried out to assess the validity of the theoretical results. Attention is focused on the influence of the effective area, the source buoyancy flux and the time during which the source is switched on.

In the absence of a source, it is shown that, by opening the vents, the pressure difference between the two zones drives the exchange flow, whose intensity, as measured by the volumetric exchange flux, Q_e, is a decreasing function of time. Two counterpart horizontal currents propagate along the bottom (top) of the light (dense) zone. Upon reflection from the end walls two internal bores are generated and propagate back toward the vent(s). In our model, a horizontal interface in each zone divides the upper layer, which is comprised of fluid having the initial density of the light zone, from the lower layer, comprised of fluid whose density is larger than that of the light zone. The time rate of change of interface height is given as a function of the volumetric exchange rate, Q_e, in (7), which itself is a function of the effective area, A^*. After the ending time, t_E defined by (12), the interface elevations are steady and Q_e is zero.

We separately consider a more involved problem in which there is an isolated source of buoyancy located at the floor of the light zone and which

supplies fluid of density ρ_c over a dimensional time interval t_s with (time-invariant) buoyancy flux F_s. The source strength Π_s, defined by (28), is the ratio of the buoyancy added by the source to the total buoyancy of the system at time $t = 0$. Two distinct flow regimes are defined: a ventilation-dominated regime with $\Pi_s < 1$ and a source-dominated regime with $\Pi_s > 1$. Particular attention is here focused on the former regime. When a source is present, there remains an exchange of mass and buoyancy between the two zones for $t > t_E$. Indeed the flow into the dense zone is characterized by one or more ascending plumes so that non-trivial stratification of density appears in both building zones for sufficiently large time.

By way of summary, note that the terminal stratification and buoyancy in either zone are not impacted by the number of open vents when $\tau_s > \tau_3$. However, the ending time, which is indicative of the evolution time-scale for h_b and h_t, is strongly influenced by N_b and N_t. These observations are especially important when buoyancy differences are due, not as we have assumed thus far to temperature differences, but rather to the presence of some noxious gas or harmful suspended particulate. In this case, knowledge of the temporal evolution of the interface heights and, equivalently, the variation of Q_e, is critical in estimating how long an occupant has to vacate a particular building zone. In terms of an attached solarium and adjacent building zone, it is obviously advantageous to have $\tau_s > \tau_3$ so as to derive the greatest possible benefit from the solar gains in the zone more likely to be inhabited by building occupants. Consistent with the results displayed in Figures 9 to 12, the impact of the source on the final buoyancy is weak for the range of parameters employed in our experiments. However, as shown by Figures 9 to 11 and consistent with Figures 3 and 4, the influence of the source parameters can be substantial even for $\Pi_s < 1$ in that the details of the density stratification can be non-trivially altered by changing F_s or t_s and this may, in turn, non-trivially impact the degree of thermal comfort experienced by those inside the building. Good agreement is observed for the evolution of the interface in each zone with average relative errors of 9.6% and 10.4% for h_b/H and h_t/H, respectively.

The current model is derived for relatively modest values of $(h + D)/H$ where h, D and H are defined by Figure 1. For larger values of h or D the flow is not completely horizontal, unidirectional and uniform. This does not necessarily limit the applicability of our model if one recalls that in systems that exploit displacement ventilation the vents should be located as near to the floor and ceiling as possible, so that the exchange of mass and buoyancy may occur over the broadest possible range of interface heights [37]. We only provided experimental results for cases where $\ell/L = 1/2$, i.e. the two zones have the same size. This scenario is generally representative, however: for $0.10 < \ell/L < 0.90$, qualitatively similar results are expected and the model can be applied straightforwardly. Cases where $\ell \ll L - \ell$ or $\ell \gg L - \ell$ indicating a significant asymmetry in the size of adjacent zones are of less architectural relevance. In these strongly asymmetrical cases, one zone is thin and tall and overturning may occur, which is associated with large scale vertical circulation rather than the filling-box process.

Acknowledgments

References

[1] Sandbach SD, Lane-Serff GF. Transient buoyancy-driven ventilation: Part 1. Modelling advection. Build Environ 2011;46:1578-1588.

[2] Axley J. Multizone airflow modeling in buildings: history and theory. HVAC&R Research 2007;13(6):907–28.

[3] Song F, Zhao B, Yang X, Jiang Y, Gopal V, Dobbs G, Sahm M. A new approach on zonal modeling of indoor environment with mechanical ventilation. Building and Environment 2008;43(3):278–86.

[4] Chen Q. Ventilation performance prediction for buildings: A method overview and recent applications. Build Environ 2009;44:848-858.

[5] Laughman CR, Nabi S, Grover P. A study of refrigerant dispersion in occupied spaces under parametric variation. In ASHRAE Annual Meeting, 2015.

[6] Kaye NB, Flynn MR, Cook MJ, Ji Y. The role of diffusion on the interface thickness in a ventilated filling box. J Fluid Mech 2010;652:195-205.

[7] Linden PF, Lane-serff GF, Smeed DA. Emptying filling boxes: the fluid mechanics of natural ventilation. J Fluid Mech 1990;212:309-335.

[8] Caulfield CP, Woods W. The mixing in a room by localized finite-mass-flux source of buoyancy. J Fluid Mech 2002;471:33-50.

[9] Kuesters AS, Woods W. The formation and evolution of stratification during transient mixing ventilation. J Fluid Mech 2010;670:66-84.

[10] Nabi S, Flynn MR. The hydraulics of exchange flow between adjacent confined building zones. Build Environ 2013;59:76-90.

[11] Nabi S, Flynn MR. Influence of geometric parameters on the eventual buoyancy stratification that develops due to architectural exchange flow. Build Environ 2014;71:33-46.

[12] Wang L, Chen Q. Evaluation of some assumptions used in multizone airflow network models. Building and Environment 2008;43(10):1671–7.

[13] Wang L, Chen Q. Validation of a coupled multizone and CFD program for building airflow and contaminant transport simulations. HVAC&R Research 2007;13(2):267–81.

[14] Megri AC, Haghighat F. Zonal modeling for simulating indoor environment of buildings: review, recent developments, and applications. HVAC&R Research 2007;13(6):887–905.

[15] Tan G, Glicksman LR. Application of integrating multi-zone model with CFD simulation to natural ventilation prediction. Energy Build 2005;37:1049–1057.

[16] Zhang Z, Chen X, Mazumdar S, Zhang T, Chen Q. Experimental and numerical investigation of airflow and contaminant transport in an airliner cabin mockup. Build Environ 2009;44(1):85–94.

[17] Jin M, Liu W, Chen Q. Simulating buoyancy-driven airflow in buildings by coarse-grid fast fluid dynamics. Build Environ 2015;85:144–152.

[18] Morton BR, Taylor GI, Turner JS. Turbulent gravitational convection from maintained and instantaneous sources. J Fluid Mech 1956;234:1-23.

[19] Baines WD, Turner JS. Turbulent buoyant convection from a source in a confined region. J Fluid Mech 1969;37:51-80.

[20] Worster MG, Huppert HE. Time-dependent density profiles in a filling box. J Fluid Mech, 1983;132:457–466.

[21] Germeles AE. Forced plumes and mixing of liquids in tanks. J Fluid Mech 1975;71:601-623. [22] Linden P. The fluid mechanics of natural ventilation. Annu Rev Fluid Mech 1999;31:201-238, 1999.

[23] Nabi S. Buoyancy-driven exchange flow with applications to architectural fluid mechanics. PhD dissertation, University of Alberta; 2014.

[24] Kaye NG, Hunt GR. Time-dependent flows in an emptying filling box. J Fluid Mech 2004;520:135-156.

[25] Benjamin TB. Gravity currents and related phenomena. J Fluid Mech 1968;31:209-248.

[26] Klemp JB, Rotunno R, Skamarock WC. On the propagation of internal bores. J Fluid Mech 1997;331:81-106.

[27] Killworth PD, Turner JS. Plumes with time-varying buoyancy in a confined region. Geophys Astro Fluid 1982;20 (3-4):265-291.

[28] Wong ABD, Griffiths RW. Stratification and convection produced by multiple turbulent plumes. Dynam. Atmos Ocean 1999;30:101-123.

[29] Tatcher TL, Wilson DJ, Wood EE, Craig MJ, Sextro RG. Pollutant dispersion in a large indoor space: Part 1 − Scaled experiments using a water-filled model with occupants and furniture. Indoor Air 2004;14: 258–271.

[30] Hunt GR, Kaye NG. Virtual origin correction for lazy turbulent plumes. J Fluid Mech 2001;435:377-396.

[31] Taylor JR. An introduction to error analysis: The study of uncertainties in physical measurements. 2nd ed. University Science Books; 1997.

[32] Drazin PG, Reid WH. Hydrodynamic Stability (Cambridge Mathematical Library). 2nd ed. Cambridge University Press; 2004.

[33] Borden Z, Meiburg E. Circulation based models for Boussinesq gravity currents. Physics Fluids 2013;25-101299-1:14.

[34] Hunt GR, Cooper P, Linden PF. Thermal stratification produced by plumes and jets in enclosed spaces. 2001;36:871:882.

[35] Kotsovinons NE. A study of the entrainment and turbulence in a plane buoyant jet. Report No. KH-R-32, California Institute of Technology, Keck Laboratory, Pasadena, Calif., Aug., 1975.

[36] Rouse H, Yih C, Humphreys H. Gravitational convection from a boundary source. Tellus 1952;4:200-210.

[37] Rooney GG, Linden PF. Strongly Buoyant Plume Similarity and 'Small-fire' Ventilation. Fire Safe J 1997;29:235-258.